

Gut microbiome modulates cytokine release syndrome and therapeutic response to CAR-T therapy in hematologic malignancies

He Huang (✉ huanghe@zju.edu.cn)

The First Affiliated Hospital, School of Medicine, Zhejiang University <https://orcid.org/0000-0002-2723-1621>

Yongxian Hu

Bone Marrow Transplantation Center, The First Affiliated Hospital, School of Medicine, Zhejiang University

Jingjing Li

State Key Laboratory for Diagnosis and Treatment of Infectious Diseases, National Clinical Research Center for Infectious Diseases, Collaborative Innovation Center for Diagnosis and Treatment of Inf

Fang Ni

The First Affiliated Hospital, School of Medicine, Zhejiang University

Zhongli Yang

Zhejiang University

Xiaohua Gui

State Key Laboratory for Diagnosis and Treatment of Infectious Diseases, National Clinical Research Center for Infectious Diseases, Collaborative Innovation Center for Diagnosis and Treatment of Inf

Zhiwei Bao

State Key Laboratory for Diagnosis and Treatment of Infectious Diseases, National Clinical Research Center for Infectious Diseases, Collaborative Innovation Center for Diagnosis and Treatment of Inf

Houli Zhao

The First Affiliated Hospital, School of Medicine, Zhejiang University

Guoqing Wei

Zhejiang University

Yiyun Wang

Zhejiang University

Mingming Zhang

The First Affiliated Hospital, School of Medicine, Zhejiang University

Ruimin Hong

The First Affiliated Hospital, School of Medicine, Zhejiang University

Linqin Wang

The First Affiliated Hospital, School of Medicine, Zhejiang University

Wenjun Wu

First Affiliated Hospital Zhejiang University

Mohamad Mohty

AP-HP, Hôpital Saint-Antoine

Amon Nagler

Hematology and Bone Marrow Transplantation Division, Chaim Sheba Medical Center, Tel-Hashomer, Israel;

Alex Chang

Shanghai YaKe Biotechnology Ltd

Marcel van den Brink

Memorial Sloan Kettering Cancer Center <https://orcid.org/0000-0003-0696-4401>

Ming D. Li

Zhejiang University

Article

Keywords: Chimeric Antigen Receptor T Cell Therapy, Multiple Myeloma, Acute Lymphocytic Leukemia, Non-Hodgkin Lymphoma, Cytokine Release Syndrome

Posted Date: July 31st, 2021

DOI: <https://doi.org/10.21203/rs.3.rs-725566/v1>

License:  This work is licensed under a Creative Commons Attribution 4.0 International License.

[Read Full License](#)

Version of Record: A version of this preprint was published at Nature Communications on September 9th, 2022. See the published version at <https://doi.org/10.1038/s41467-022-32960-3>.

Abstract

Chimeric antigen receptor (CAR)-T cell therapy has emerged as a promising immunotherapeutic treatment for hematologic malignancies. By comparing the diversity and composition of the gut microbiome during different stages of CAR-T therapy, significant changes were detected, not only in patients with relapsed/refractory multiple myeloma (MM; n = 43), but also in those with acute lymphocytic leukemia (ALL; n = 23) and non-Hodgkin lymphoma (NHL; n = 12). Analysis of treatment responses revealed significant temporal differences in diversity and abundance of *Bifidobacterium*, *Prevotella*, *Sutterella*, and *Collinsella* between MM patients in complete remission (n = 24) and those in partial remission (n = 11). Furthermore, we found that patients with severe cytokine release syndrome (CRS) exhibited higher abundance of *Bifidobacterium*, *Leuconostoc*, *Stenotrophomonas*, and *Staphylococcus*. This study has important implications for understanding the biological role of the microbiome in the CAR-T treatment of patients with hematologic malignancies (ChiCTR1800017404).

Introduction

B-cell-derived hematologic malignancies, including acute lymphoblastic leukemia (B-ALL), non-Hodgkin lymphoma (B-NHL), and multiple myeloma (MM), carry a high probability of relapse after conventional chemotherapy¹. With novel therapeutic strategies incorporating monoclonal antibodies, bispecific T-cell engager (BiTE) antibodies, and hematopoietic stem cell transplantation (HSCT), treatment outcomes have greatly improved^{2,3,4}. However, some patients progress to relapsed/refractory (r/r) status, with a poor prognosis⁵. The 5-year overall survival (OS) rate generally is < 10% with a median OS of 3–6 months for patients with r/r B-ALL^{6,7}. The complete response (CR) rate is 7% with a median OS of 6.2 months for r/r diffuse large B-cell lymphoma (DLBCL)⁸. For r/r MM patients, the 1-year OS is about 40%⁹. There is an urgent need to explore novel treatment strategies for these malignancies.

Chimeric antigen receptor (CAR) T-cell therapy (approved by the U.S. Food and Drug Administration) recently emerged as promising for r/r B-ALL, DLBCL, and mantle cell lymphoma (MCL)^{10,11,12}. In multiple myeloma, investigations targeting the B-cell maturation antigen (BCMA) yielded encouraging outcomes with reversible toxic effects such as cytokine release syndrome (CRS) and pancytopenia^{13,14,15,16,17}. However, the efficacy and toxicity have been inconsistent. No biomarker has been identified that predicts outcome and associated toxicities after CAR-T in patients.

Several studies have reported that the differences in diversity and composition of the gut microbiome might influence cancer immunotherapy response^{18,19,20,21}. After analyzing fecal samples from 43 melanoma patients treated with anti-programmed cell death 1 protein (PD-1) immunotherapy, significantly higher alpha diversity and abundance of Clostridiales/Ruminococcaceae were found in responders, whereas Bacteroidales were significantly enriched in non-responders¹⁹. In hematologic malignancies, intestinal bacteria also modulate the risk of graft-versus-host disease (GVHD) and infection after allogeneic hematopoietic stem cell transplantation (allo-HSCT). Greater bacterial diversity

and abundance of the genus *Blautia* were associated with reduced GVHD-related death and improved OS^{22, 23}. However, no study has shown a potential role for the intestinal microbiota in the efficacy and toxicity of CAR-T therapy for B-cell malignancies.

The primary aims of this study were to understand the intestinal microbiome changes in patients with r/r B-cell-derived hematologic malignancies undergoing CAR-T cell treatment and to investigate associations of the microbiota with clinical responses and CRS severity. Finally, the potential of the gut microbiome to predict treatment outcomes and CRS severity was explored.

Results

Patient cohorts

A total of 92 patients with r/r B-cell-derived hematologic malignancies were screened. Ten patients were not eligible for inclusion. Another four patients were excluded because of lack of sufficient 16S sequencing depth. Thus, MM (n = 43), B-ALL (n = 23), and B-NHL (n = 12) patients were included (Fig. 1A).

The median age of the MM patients was 59 (range 39–75) years, and 55.8% were male (Table 1). The median number of prior lines of therapy was 4 (range 2–8), with all receiving proteasome inhibitor therapy and 95.3% immunomodulatory agents. At enrollment, 39.5% had received autologous stem cell transplantation, and 55.8% had extramedullary disease(s).

Table 1
 Baseline characteristics of multiple myeloma patients included in final fecal
 microbiome analyses cohorts.

| | Total N = 43(%) |
|--|----------------------------|
| Age | 59 |
| Median | 39–75 |
| Range | |
| Gender | 24 (55.8) |
| Male | 19 (44.2) |
| Female | |
| Number of prior lines of therapy | 4 |
| Median | 2–8 |
| Range | |
| CAR-T cell dose(×10 ⁶ /kg) | 4.4 |
| Median | 1.2–6.9 |
| Range | |
| Autologous stem cell transplantation | 26 (60.5) |
| No | 17 (39.5) |
| Yes | |
| Extramedullary disease | 19 (44.2) |
| No | 24 (55.8) |
| Yes | |
| Prior PI therapy | 0 |
| No | 43 (100) |
| Yes | |
| Prior IMiD therapy | 2 (4.7) |
| No | 41 (95.3) |
| Yes | |
| PI, Proteasome inhibitors (Bortezomib/Carfilzomib/Ixazomib). | |
| IMiD, immunomodulatory agent (Lenalidomide/Thalidomid/Pomalidomide). | |

Three months after infusion of a median dose of $4.4 \times 10^6/\text{kg}$ (range $1.2\text{--}6.9 \times 10^6/\text{kg}$) of BCMA CAR-T cells, 55.8%, 14%, and 25.5% of patients had a complete remission (CR), very good partial response (VGPR), or partial response (PR), respectively. All 43 MM patients showed CRS, grade 1 in 8 patients (18.6%), grade 2 in 16 (37.2%), and grade 3 in 19 (44.2%). No higher grade was observed (Fig. 1D). Two patients died: one from sepsis caused by *Pseudomonas aeruginosa* and the other from intracranial hemorrhage (Fig. 1D). Both the BCMA CAR-T/CD3⁺ T-cell percentages in peripheral blood (PB) and serum concentrations of interleukin (IL)-10 and interferon (IFN)- γ increased during CRS and differed significantly in the CR and PR groups (Fig. 1E). Patients' temperature and C-reactive protein (CRP), ferritin, and lactic dehydrogenase (LDH) concentrations were elevated, and IL-6 and IFN- γ concentrations were significantly different in grade 3 vs grade 1 CRS (Fig. 1F **and Supplementary Fig. 1A-C**). The serum immunoglobulins (IgG, IgA) and immunoglobulin κ and λ light chain concentrations decreased dramatically after CAR-T (**Supplementary Fig. 1D-F**). Figure 1G shows the differences of positron emission tomography-computed tomography (PET-CT) scans and plasma cells detected by Wright's stain of a bone marrow smear (43.5% vs. 0), as well as flow cytometry (68.9% vs. 0) of bone marrow cells before and after CAR-T infusion for a representative subject.

Changes in the intestinal microbiome during CAR-T cell therapy

To detect changes in the gut microbiota during CAR-T, we collected fecal samples from each patient at five times (FCa, FCb, CRSa, CRSb, and CRSc; Fig. 1C), where FCa denotes the baseline when patients were first enrolled; FCb after chemotherapy; CRSa after CAR T-cell infusion but before the onset of CRS; and CRSb and CRSc the peak and during the recovery phase of CRS, respectively.

We first evaluated the diversity of the gut microbiota in all subjects during CAR-T cell therapy. There was a significant decrease in diversity (measured by the Simpson index) during and after CRS (at CRSb and CRSc) compared with baseline (Fig. 2A). This decrease was observed in the microbiome of patients receiving CAR-T therapy for r/r ALL (**Supplementary Fig. 4A**) or r/r NHL (**Supplementary Fig. 4B**). Refer to **Supplementary Table 1** for details on the characteristics of r/r B-ALL and B-NHL patients. To further assess the similarity of composition between different therapy stages, we performed pairwise Spearman correlation analysis of operational taxonomic unit (OTU) level bacterial abundance (Fig. 2B) and found that stronger correlations emerged during the early stages with a ρ value of 0.71, 0.73, and 0.68, respectively, at FCa, FCb, and CRSa. Correlations between late stages (CRSb and CRSc) and early stages were weaker, suggesting that changes in microbiome composition might be related to CRS.

We next explored community structure and temporal shift of bacterial abundance at multiple taxonomic levels during CAR-T therapy. In myeloma, bacterial communities were dominated by Firmicutes and Bacteroidetes at the phylum level (Fig. 2C) and characterized by significant enrichment of Firmicutes and depletion of Bacteroidetes at the last two timepoints (Fig. 2D, E and **Supplementary Fig. 4C**). By applying the longitudinal analysis in the Qiime2 microbiome analysis platform, we detected changes in the gut microbial communities at taxonomic levels from phylum to genus (Fig. 2F **and Supplementary Table 2**).

We further employed a negative binomial (NB) regression model-based time-course analysis to identify genera with significant temporal changes (**Supplementary Table 3**). Five genera were detected by both Qiime2 and maSigPro procedures, which included increases in *Enterococcus*, *Lactobacillus*, and *Actinomyces* and decreases in *Bifidobacterium* and *Lachnospira* (**Supplementary Fig. 4D**). Most changes were aggravated during the late stages. Moreover, by checking changes in the five genera in ALL and NHL patients, we observed consistent shift trends in NHL (four genera; **Supplementary Fig. 4E**) and ALL (two genera; **Supplementary Fig. 4F**), respectively.

Association between microbial communities and clinical response to CAR-T therapy

We next determined whether microbial compositions or changes were associated with the response to CAR-T. Because we wanted to identify maximum differences and only six subjects presented in the VGPR group, we performed comparisons only between the CR and PR groups.

Notable differences in microbial alpha and within-sample diversity were observed in patients with CR and PR (Fig. 3A, B). Although no differences were detected at baseline, PR patients descended more dramatically in alpha diversity and had significantly lower Shannon indices than CR patients after CAR-T infusion (Fig. 3A). As the degree of differences between CR and PR groups changed across therapeutic stages, we characterized the periods with greater differences by summarizing the amount of CR/PR-enriched OTU at each timepoint. The most pronounced differences occurred at CRSb (Fig. 3C).

To explore longitudinal differences between CR and PR across all therapeutic stages, we identified OTU features with differential dynamic profiles by applying negative binomial regression-based time-course differential analysis with the maSigPro package. In total, 125 OTUs were found to have differential time-course patterns between CR and PR patients (Fig. 3D and **Supplementary Table 4**). The significant OTUs were further grouped into three clusters according to profiles of their abundance. Most of these OTUs were in clusters 1 and 2 (Fig. 3E). Cluster 1, characterized by enrichment in the CR group, was comprised mainly of OTUs, which belong to the phyla Firmicutes and Bacteroidetes and the orders Clostridiales and Bacteroidales. Cluster 2 was comprised of OTUs from a broader taxonomy, which included the orders Clostridiales, Bacteroidales, Lactobacillales, and Actinomycetales (Fig. 3F).

We identified 30 genera with differential time-course patterns in patients with CR and PR after CAR-T (**Supplementary Table 5**). To explore these differences further, we divided the therapeutic period into before and after CAR-T infusion and performed genus-level class comparisons using linear discriminant analysis (LDA) of effect size (LEfSe)²⁴. We detected 34 genera with differences in abundance in the CR and PR groups (Fig. 4A). Eighteen genera were detected by both procedures (**Supplementary Fig. 5A**). Consistent with the results from OTU-level pattern analysis, most of the significant genera such as *Faecalibacterium*, *Roseburia*, and *Ruminococcus* were enriched in CR patients after CAR-T. The genera *Bifidobacterium*, *Prevotella*, *Sutterella*, *Oscillospira*, *Paraprevotella*, and *Collinsella* had a higher abundance in CR versus PR patients both before and after CAR-T (Fig. 4A and **Supplementary Fig. 5B**). We also took patients with VGPR into consideration and analyzed the above-mentioned genera before

and after CAR-T infusion. The bacterial abundance in VGPR patients fell somewhere between CR and PR patients, but no statistical significance was evident for most of genera (Fig. 4B and **Supplementary Fig. 5D**).

To explore whether early bacterial abundance was indicative of therapeutic response, we used RF feature selection to identify key discriminatory genera for responses²⁵. By defining the stages before CAR-T infusion as early, we applied feature selection procedures individually at both baseline (FCa) and post-chemotherapy (FCb) and identified gut microbiome signatures comprising 8 and 14 discriminatory genera separately for baseline and post-chemotherapy (Fig. 4C, D and **Supplementary Fig. 5C**). The area under the receiver operating characteristic curve (ROC) of the two RF models using these discriminatory features was 0.73 and 0.85, respectively (Fig. 4E, F). *Prevotella*, *Collinsella*, *Bifidobacterium*, and *Sutterella* were enriched in CR versus PR both before and after CAR-T infusion and were identified by RF analysis as significant at baseline and post-chemotherapy. This indicates potential associations between these genera and the response to CAR-T.

We also checked the abundance of these genera in r/r NHL and ALL patients. In NHL, *Faecalibacterium*, *Bifidobacterium*, and *Ruminococcus* were significantly (or almost significantly) enriched in CR versus PR and in patients not having a remission (NR), consistent with our results in myeloma (**Supplementary Fig. 5E**). However, for ALL, we observed enrichment of *Bifidobacterium*, *Roseburia*, and *Collinsella* in NR (**Supplementary Fig. 5F**), which differed from the results for MM and NHL but might be determined by the small NR sample.

To further demonstrate the association between these taxa and outcome, we assessed progression-free survival (PFS) following CAR-T therapy. By stratifying patients by tertile of bacterial abundance, we observed that for *Sutterella*, patients in the highest-abundance tertile had significantly prolonged PFS (Fig. 4G). Even after stratification by timepoints, this association remained significant (**Supplementary Fig. 6A**). However, for genus *Faecalibacterium*, which was reported to be significantly associated with PFS and anti-PD-1 therapy¹⁹, we did not observe an association (**Supplementary Fig. 6B, C**).

We performed pathway analysis using Phylogenetic Investigation of Communities by Reconstruction of Unobserved State (PICRUSt) and identified significant changes in amino acid metabolism (Fig. 4H), important for immune function²⁶. For example, CR patients had higher lysine biosynthesis, whereas PR patients had higher lysine degradation. Glutathione metabolism, which can have different effects on functional immunity²⁷, was increased in PR patients. Peptidoglycans biosynthesis was increased in CR versus PR patients. Bacteria-derived peptidoglycans are an important pathogen-associated molecular pattern (PAMP) that can activate inflammatory signaling pathways and stimulate immune responses²⁸.

Associations between gut microbiome and CRS

Manifestations of severe CRS, namely high fever and greater amounts of cytokines, typically develop within several days after CAR-T cell infusion and may cause death if untreated²⁹. We scaled CRS from level 1 to 5³⁰. To analyze associations between bacterial communities associated with CRS, we

compared patients with severe (level 3) versus mild (level 1) CRS and severe and moderate CRS (level 2). We found 146 OTUs with different time patterns in the severe and mild groups (**Supplementary Fig. 7** and **Supplementary Table 6**), and 99 OTUs with different patterns in the severe and moderate CRS groups (**Supplementary Fig. 8** and **Supplementary Table 7**). The profiles of the OTU clusters for the comparisons were similar, with OTUs in clusters 1 and 3 having a higher abundance during late therapy in patients with severe versus mild CRS (**Supplementary Fig. 7B** and **Supplementary Fig. 8B**). By analyzing associations between CRS grade and taxa at the genus level, we identified signatures discriminating severe from mild CRS, including decreases in amount of *Bifidobacterium* and *Leuconostoc* in patients with severe CRS (**Fig. 5A** and **Supplementary Table 8**). *Bifidobacterium* was increased in patients with worse CRS, not only during the window of CRS, but also at early stages (**Fig. 5A, B**). *Leuconostoc* was significantly enriched during the window in patients with high CRS grade (**Fig. 5A, B**). In addition, the abundance of *Stenotrophomonas* and *Staphylococcus* differed severe vs moderate CRS during the window (**Supplementary Fig. 8D** and **Supplementary Table 9**).

Comparisons of KEGG pathways across CRS groups showed that the gut microbiome of patients with severe CRS had high metabolism or biosynthesis related to inflammatory compounds, including several pathways associated with amino acid synthesis and metabolism, purine metabolism, lipoic acid metabolism, and biosynthesis of lipopolysaccharide and peptidoglycan (**Supplementary Fig. 9** and **Supplementary Fig. 10**).

Primary inflammatory markers of CRS are cytokines, such as IL-6, IL-2, IL-10, interferon gamma (IFN- γ), and tumor necrosis factor- α (TNF- α). Various cytokines are elevated in the serum of patients experiencing CRS after CAR-T cell infusion³¹. By assessing serum cytokine concentrations and immune cell numbers during CAR-T, we observed significantly increased amounts of serum inflammatory cytokines (IL-6, CRP, IFN- γ , D-dimer, ferritin) but low numbers of immune cells (monocytes, lymphocytes, neutrophils, leukocytes) in severe CRS (**Fig. 5C**). We also compared serum cytokine concentrations and immune cell numbers in CR and PR, observing significant differences for many of them (see **Supplementary Fig. 11A**).

To explore further associations between the gut microbiome and CRS during CAR-T therapy, we determined whether serum cytokine concentrations and numbers of PB immune cells correlated with the abundance of gut microorganisms (**Fig. 5D**). The abundance of the genus *Leuconostoc*, previously linked to CRS grade, correlated positively with ferritin and D-dimer concentrations. The abundance *Bifidobacterium* correlated significantly negatively with PB monocytes (**Fig. 5E**). We also found a correlation between inflammatory markers and bacteria associated with the clinical response and PFS. For example, *Sutterella* correlated negatively with serum concentrations of CRP and D-dimer (**Supplementary Fig. 11B**). *Prevotella* correlated negatively with the number of multiple PB immune cells but positively with the serum D-dimer concentration (**Supplementary Fig. 11B**). *Faecalibacterium* correlated negatively with the serum concentrations of D-dimer and IFN- γ (**Supplementary Fig. 11B**).

Discussion

Although several studies have revealed the critical role of the gut microbiome in treatment responses and survival after administration of another important immunotherapy – immune checkpoint inhibitor (e.g., PD-1, PD-L1) therapy²⁰, no study has reported on the association between the gut microbiome and CAR-T therapy. In this study, we describe the changes of the gut microbiome during CAR-T therapy and associations with treatment responses and CRS severity in CAR-T-treated patients with B-cell malignancies.

Some of the bacterial genera with differences in abundance in CR versus PR patients have been reported to be involved in the regulation of the immune response, including to immunotherapy. *Faecalibacterium*, reported to enhance antitumor immune responses and survival after anti-PD-1 therapy in melanoma^{19,32}, was in this study associated with CR. Multiple species within the genera *Bifidobacterium* and *Collinsella* increased in responders to anti-PD-1 therapy for melanoma³³, resulting in depleted peripherally derived colonic regulatory T cells, increased Batf3-lineage dendritic cells (DCs), and augmented T-helper 1 cell (Th1) responses and thus better immune-mediated tumor control³⁴. Here, we observed an increased abundance of these two bacteria in CR patients, suggesting a similar response-associated effect of these taxa on the immune system across cancer types and therapeutic strategies.

Nevertheless, some taxa might have effects that are specific for cancer or therapy types. For example, high abundance of genus *Sutterella* was associated with both CR and prolonged survival after CAR-T therapy. However, previous studies reported higher numbers of *Sutterella* in non-responders versus responders in non-small-cell lung cancer (NSCLC) treated with nivolumab³⁵. Besides, in this study, we observed contradictory results for the genus *Bifidobacterium*, *Roseburia*, and *Collinsella* in three types of hematologic malignancy (**Supplementary Fig. 2F**). This indicates a potentially distinct involvement or function of some bacteria in different cancer types and treatments. But these findings require confirmation in studies with larger cohorts.

Gut microbial communities contribute to inter-individual variation in cytokine responses³⁶. We propose that gut microbes are related to the intensity of CRS during CAR-T therapy. *Bifidobacterium*, *Leuconostoc*, *Stenotrophomonas* and *Staphylococcus* were enriched in myeloma patients with severe CRS. Additional studies also demonstrated an association between these microbes and cytokine production. Previous research showed that *Bifidobacterium* correlated with the production of multiple cytokines (e.g., IFN- γ) in a stimulus-specific pattern³⁶. The opportunistic pathogen *Stenotrophomonas maltophilia* can stimulate the expression of proinflammatory cytokine and chemokine genes in *vitro* and *in vivo*^{37,38}. Moreover, superantigens, a family of potent exotoxins produced by *Staphylococcus*, were could eliciting T-cell-driven CRS during treatment with CAR T-cells, T-cell agonistic antibodies, immune check point inhibitors, haploidentical HSCT, and other therapies³⁹.

The mechanisms through which gut microbes modulate host immunity are largely unknown. Gut microbial communities modulate host defenses mainly through the release of intermediary metabolites rather than by direct interaction between specific microorganisms and immune cells³⁶. Multiple bioactive

gastrointestinal metabolites produced by gut microbes, such as amino acids, short-chain fatty acids (SCFAs; e.g., butyrate), and bile acids, exert immunomodulatory functions through immune cell metabolic reprogramming or transcriptional and epigenetic modulation of immune-related genes²⁶. Lipopolysaccharide (LPS) from some pathogens is a well-known endotoxin that can stimulate the release of a variety of cytokines/chemokines^{40,41}. Peptidoglycans in bacterial cell walls are a conserved PAMP that trigger innate inflammatory responses throughout the body⁴².

In addition to myeloma, CAR-T therapy has been applied other blood cancers and solid tumors. The link between the gut microbiome and different cancer types needs to be studied systematically. Our research describes associations between changes in the gut microbiome of CAR-T patients and clinical responses and survival. This will open an avenue for investigating the interaction of the gut microbiome and CAR-T cells and lead to novel ways to improve the therapeutic efficacy of CAR-T therapy by targeting the gut microbiome.

As one of the most prominent treatment strategies for hematologic malignancies, CAR-T cell therapy has recently received great attention. Here for the first time, we found that the dynamic changes in the gut microbiome correlated significantly with therapeutic response and CRS during CAR-T treatment of hematologic malignancies (B-ALL, B-NHL, and MM). These findings will aid the development of novel biomarkers for predicting treatment outcome and CRS severity, thereby optimizing the management of these patients while reducing potential toxicities.

Methods

METHODS

Study design and protocol

The study was approved by the Institutional Review Board of the First Affiliated Hospital, School of Medicine, Zhejiang University and was registered in the Chinese Clinical Trial Registry (ChiCTR1800017404). All patients provided written informed consent for participation in accordance with the guidelines of the Declaration of Helsinki and signed agreement for collection and analysis of microbiome samples.

Patient inclusion criteria were: (1) age < 75 years; (2) relapsed or refractory BCMA-positive MM before CAR-T cell treatment; and (3) expected survival > 12 weeks and adequate performance status and organ function to tolerate treatment. Exclusion criteria were: (1) pregnancy or lactation; (2) having received systemic (except inhaled) steroids in the previous 2 weeks or gene therapies; (3) having medical conditions such as severe mental illness, clinically significant cardiovascular disease, severe renal or hepatic dysfunction, or active infection; and (4) any conditions that might increase treatment risks. Patient information and the methods related to two types of cancer (ALL and NHL) are presented in the Supplementary Materials.

Peripheral blood mononuclear cells (PBMCs) were obtained from each patient by leukapheresis for CAR-T cell preparation. The purified CD3⁺ T cells were transduced with lentiviral vector to express BCMA CAR (Fig. 1B). Then the engineered T cells were expanded *ex vivo* under interleukin-2 stimulation. All patients received lymphodepletion with fludarabine (30 mg/m² of body surface area daily on days - 4, -3, and - 2) and cyclophosphamide (500 mg/m² daily on days - 3 and - 2) followed by an infusion of BCMA CAR-T cells on day 0. The primary response outcome, defined by the guidelines from the International Myeloma Working Group (IMWG) as a complete response (CR), very good partial response (VGPR), or partial response (PR) in the third month after CAR-T treatment^{43,44}. CRS was graded by the Lee criteria³⁰.

Microbiome sample collection and restoration

Gut microbiome samples were collected at five timepoints (Fig. 1C). All fecal samples were collected with the GUHE Flora Storage kit (Zhejiang Hangzhou Equipment Preparation 20190682, GUHE Laboratories, Hangzhou, China), which maintains microbial DNA stability at room temperature for as long as one month. All samples were frozen at -80°C prior to DNA extraction. The stages of FCa, FCb, and CRSa were defined as early stages and CRSb and CRSc as late stages. The CRS grade 1 was defined as Mild, CRS grade ≤ 2 as Moderate, and CRS grade ≥ 3 as Severe.

Assessment of serum cytokine concentrations

All blood samples were stored at 4°C until centrifugation at 5000 rpm for 6 min. The supernatant liquids were quantified with the BD Cytometric Bead Array Human Th1/Th2/Th17 Cytokine Kit and its corresponding software (BD Biosciences) according to the manufacturer's instructions.

Assessment of CAR-T cell expansion and persistence

Serial PB samples were collected in BD Vacutainer K₂EDTA tubes (BD Biosciences) before and after CAR-T cell infusion. The expansion of CAR-T cells *in vivo* was determined by detecting the CAR-T ratio continuously in PB as described^{45,46}. BCMA CAR-T expression was assessed using biotin-SP-conjugated F(ab')₂ fragment goat anti-mouse IgG, F(ab')₂ fragment-specific antibody, and the secondary staining reagent streptavidin-FITC (BioLegend, 405202) or streptavidin-PE (BioLegend,405204).

DNA Extraction

Total bacterial genomic DNA samples were extracted using the MO BIO PowerSoil DNA Isolation Kit (MO BIO Laboratories, Carlsbad, CA, USA). The quantity and quality of extracted DNA was assessed using both the NanoDrop ND-1000 Spectrophotometer (Thermo Fisher Scientific, Waltham, MA, USA) and agarose gel electrophoresis.

Bacterial 16S rRNA gene sequencing

The V4 region of the 16S rRNA gene was amplified with bacterial universal primers: 515F (5'-GTGCCAGCMGCCGCGGTAA-3') and 806R (5'-GGACTACH VGGGTWTCTAAT-3'). The primers used for amplification contain adapters for the HiSeq platform and single-end barcodes allowing pooling and

demultiplexing sequences of PCR products. Amplified sequences were purified with AMPure XP beads (Agencourt, Inc, Beverly, Manchester, MA, USA) and AxyPrep DNA Gel Extraction Kit (Axygen, Inc, Union City, CA). Qualified PCR products were sequenced with the HiSeq platform (Illumina, Inc, San Diego, CA, USA) using the 2 × 150-bp paired-end sequencing protocol.

Amplicon data processing

Sequenced reads were demultiplexed according to barcodes. Paired-end reads were merged with the *fastq_mergepairs* command from VSEARCH v. 2.4.4⁴⁷. The minimum length of overlap between paired-end reads was set to 5. Merged reads were then imported into Qiime2 (v. 2020.2)⁴⁸. Jointed reads were processed by the *qiime quality-filter q-score-joined* command to filter sequences with low-quality scores. Sequences were denoised with the *Deblur* workflow⁴⁹. Amplicon sequence variants (ASVs) were summarized with the *feature-table summarize* command. To calculate phylogenetic diversity, a rooted phylogenetic tree was constructed using the *align-to-tree-mafft-fasttree* pipeline from the *q2-phylogeny* plugin within Qiime2. The pipeline performed a multiple sequence alignment of the ASV sequences and then masked the alignment to remove positions that are highly variable. The masked alignment was used to generate a phylogenetic tree by *FastTree* program⁵⁰. Alpha and beta diversity matrices were generated through the *q2-diversity* plugin using the above-mentioned ASV feature table and rooted phylogenetic tree. *De novo* clustering of ASVs was performed with the *cluster-features-de-novo* command within *vsearch* plugin⁴⁷. Input features were collapsed at 97% identity, resulting in new OTU features that are clusters of the ASV features. Representative OTU sequences were then annotated with pre-trained Naive Bayes classifier trained on the Greengenes 13_8 99% OTU database using the *feature-classifier* plugin⁵¹. The sequences used for training were trimmed to include only the V4 region. Taxonomic composition was summarized with the *collapse* method from the *taxa* plugin within Qiime2.

Functional prediction

We used the OTU feature table generated from Qiime2 to predict microbial community function with PICRUST2⁵². The PICRUST2 algorithm performed functional prediction based on marker gene sequencing profiles and searched for the most closely related organisms with annotated genomes to infer gene contents per OTU. Gene family abundance per sample was summarized and grouped into KEGG orthologs (KOs). To facilitate the interpretation of functional results, KOs were further summarized into KEGG pathways on the basis of structured pathway mappings. For differential pathway analysis, we applied the two-sided Welch's *t*-test to identify discriminative KEGG pathways concerning clinical responses (PR versus CR) and CRS level (level 1 versus level 3).

Bioinformatics and statistical analysis

Comparisons of alpha diversity and taxonomic abundances between two groups were conducted with the Wilcoxon rank-sum test, while comparisons among three or more groups were conducted using the Kruskal-Wallis rank-sum test. For beta diversity analysis, a PCoA plot was generated with weighted

Unifrac distances. To test the significance of between-sample diversity alternation, permutational analysis of variance (PERMANOVA) was performed with the *adonis* function within the R package *vegan*.

The *feature-volatility* plugin⁵³ within Qiime2 was applied to implement longitudinal analysis to identify features that are associated with therapy stages. In this pipeline, supervised learning regressor was used to identify important features and assess their ability to predict therapy states. Unclassified taxonomic features, features absent in more than 90% of all samples, and features with low abundance (< 0.01%) were all excluded from the analysis. Net average change scores and importance scores, which denote the correlation between input features and therapy stages, were exported and visualized in a volcano plot. Only features with net average change scores more than 0.2% and importance scores within the first tertile of distribution were retained.

For time-course differential analysis, the R package *maSigPro*^{54, 55} was used to find taxonomic features with significant temporal changes and significant differences between experimental groups (e.g., clinical response and CRS grade groups). Specifically, the *maSigPro* algorithm defined a generalized regressive model by dummy variables followed by two regression steps: the first one selects features with non-flat profiles by the least-squared technique and the second step creates best regression models for each feature by using stepwise regression to identify features with different profiles between experimental groups. We used as input, the normalized relative abundance (scaled to 100 million) and excluded features that did not occur in more than 90% of all samples. We employed a negative binominal regressive model for the microbial counts data and ran *maSigPro* on therapy stages with a degree of 4. All features with a significant group difference were exported. The significant features were further clustered together using the *hclust* function method according to the patterns of their relative abundance. For each cluster, a median profile and fitted curve of all included features were summarized to visualize the profile pattern.

The LAD effect size (LEfSe) algorithm²⁴ was employed to identify differentially abundant features between groups (e.g., between clinical response and CRS grade). The method first detected features with significant differential abundance using the non-parametric factorial Kruskal-Wallis rank-sum test with pre-defined α of 0.05. Significant features were then used to build a Linear Discriminant Analysis (LDA) model for estimating the effect size of each differentially abundant feature. The LDA score threshold for discriminative features was set to 2.0.

To identify early predictive biomarkers with respect to clinical response (PR vs. CR), we implemented a random forest (RF) feature selection procedure within the R package *caret*. The recursive feature elimination (RFE) algorithm with 5-fold cross validation was applied for feature selection. An optimized number of feature sets was determined by performance of 5-fold cross validation. To depict the receiver operating characteristic (ROC) curve and calculate the area under the curve (AUC), the *pROC* package was utilized.

For progression-free survival (PFS) analysis, subjects were classified as high, medium, or low based on tertiles of the distribution of specific taxa abundance (e.g., genus *Sutterella*). Time to progression was defined as the interval (in days) from the date of CAR T-cell infusion to the date of disease progression. Survival curves were estimated using the Kaplan-Meier product-limit method and compared using the log-rank test within the R package *survminer*.

We applied Spearman's rank-order correlation to test the association between bacterial abundance and concentration of immune cells and inflammatory factors. Only genus-level features deemed to be associated with clinical response and CRS grades were included in this analysis. Associations with an absolute value of correlation coefficient higher than 0.2 and FDR less than 0.2 were depicted using Cytoscape⁵⁶.

Declarations

Competing interests

The authors declare no competing financial interests.

Data and materials availability

For original data, please contact the corresponding author.

Author contributions

H.H. designed and supervised the clinical study; H.C., Y.Z. and Y.W. supervised the CAR T-cell production; Y.H., W.W., M.Z., G.W., R.H., and L.W. collected clinical data; M.L., J.L., F.N., Z.Y., H.G., and W.B. analyzed data, wrote and revised the manuscript; J.L., Z.Y. and H.G. performed statistical analyses; Y.H., W.W., M.Z., G.W., R.H., and L.W. enrolled patients and took care of the patients; H.H., M.M., A.N., and D.B. revised the manuscript.

Acknowledgements

This study was supported by the National Natural Science Foundation of China (grant No. 81730008, 81770201), Key Project of Science and Technology Department of Zhejiang Province (grant No. 2019C03016), China Precision Medicine Initiative (2016YFC0906300), Research Center for Air Pollution and Health of Zhejiang University, and the State Key Laboratory for Diagnosis and Treatment of Infectious Diseases, The First Affiliated Hospital of Zhejiang University. We thank Dr. David Bronson and Mrs. Judith Gunn Bronson of Stem Line Publishing Services, Inc. for their editing of this manuscript.

References

1. Stephenson R, Singh A. Drug discovery and therapeutic delivery for the treatment of B and T cell tumors. *Adv Drug Deliv Rev* **114**, 285–300 (2017).
2. Habermann TM, *et al.* Rituximab-CHOP versus CHOP alone or with maintenance rituximab in older patients with diffuse large B-cell lymphoma. *J Clin Oncol* **24**, 3121–3127 (2006).
3. Goebeler ME, *et al.* Bispecific T-Cell Engager (BiTE) Antibody Construct Blinatumomab for the Treatment of Patients With Relapsed/Refractory Non-Hodgkin Lymphoma: Final Results From a Phase I Study. *J Clin Oncol* **34**, 1104–1111 (2016).
4. Lokhorst HM, *et al.* Targeting CD38 with Daratumumab Monotherapy in Multiple Myeloma. *N Engl J Med* **373**, 1207–1219 (2015).
5. Sonneveld P. Management of multiple myeloma in the relapsed/refractory patient. *Hematology Am Soc Hematol Educ Program* **2017**, 508–517 (2017).
6. Gokbuget N, *et al.* Outcome of relapsed adult lymphoblastic leukemia depends on response to salvage chemotherapy, prognostic factors, and performance of stem cell transplantation. *Blood* **120**, 2032–2041 (2012).
7. Kantarjian HM, *et al.* Defining the course and prognosis of adults with acute lymphocytic leukemia in first salvage after induction failure or short first remission duration. *Cancer* **116**, 5568–5574 (2010).
8. Crump M, *et al.* Outcomes in refractory diffuse large B-cell lymphoma: results from the international SCHOLAR-1 study. *Blood* **130**, 1800–1808 (2017).
9. Kumar SK, *et al.* Risk of progression and survival in multiple myeloma relapsing after therapy with IMiDs and bortezomib: a multicenter international myeloma working group study. *Leukemia* **26**, 149–157 (2012).
10. Maude SL, *et al.* Chimeric antigen receptor T cells for sustained remissions in leukemia. *N Engl J Med* **371**, 1507–1517 (2014).
11. Maude SL, *et al.* Tisagenlecleucel in Children and Young Adults with B-Cell Lymphoblastic Leukemia. *N Engl J Med* **378**, 439–448 (2018).
12. Neelapu SS, *et al.* Axicabtagene Ciloleucel CAR T-Cell Therapy in Refractory Large B-Cell Lymphoma. *N Engl J Med* **377**, 2531–2544 (2017).
13. Zhao WH, *et al.* A phase 1, open-label study of LCAR-B38M, a chimeric antigen receptor T cell therapy directed against B cell maturation antigen, in patients with relapsed or refractory multiple myeloma. *J Hematol Oncol* **11**, 141 (2018).
14. Raje N, *et al.* Anti-BCMA CAR T-Cell Therapy bb2121 in Relapsed or Refractory Multiple Myeloma. *N Engl J Med* **380**, 1726–1737 (2019).
15. Brudno JN, *et al.* T Cells Genetically Modified to Express an Anti-B-Cell Maturation Antigen Chimeric Antigen Receptor Cause Remissions of Poor-Prognosis Relapsed Multiple Myeloma. *J Clin Oncol* **36**, 2267+ (2018).

16. Xu J, *et al.* Exploratory trial of a biepitopic CAR T-targeting B cell maturation antigen in relapsed/refractory multiple myeloma. *Proc Natl Acad Sci U S A* **116**, 9543–9551 (2019).
17. Ali SA, *et al.* T cells expressing an anti-B-cell maturation antigen chimeric antigen receptor cause remissions of multiple myeloma. *Blood* **128**, 1688–1700 (2016).
18. Zitvogel L, Ma Y, Raoult D, Kroemer G, Gajewski TF. The microbiome in cancer immunotherapy: Diagnostic tools and therapeutic strategies. *Science* **359**, 1366–1370 (2018).
19. Gopalakrishnan V, *et al.* Gut microbiome modulates response to anti-PD-1 immunotherapy in melanoma patients. *Science* **359**, 97–103 (2018).
20. Yi M, *et al.* Gut microbiome modulates efficacy of immune checkpoint inhibitors. *J Hematol Oncol* **11**, 47 (2018).
21. Vetizou M, *et al.* Anticancer immunotherapy by CTLA-4 blockade relies on the gut microbiota. *Science* **350**, 1079–1084 (2015).
22. Staffas A, Burgos da Silva M, van den Brink MR. The intestinal microbiota in allogeneic hematopoietic cell transplant and graft-versus-host disease. *Blood* **129**, 927–933 (2017).
23. Jenq RR, *et al.* Intestinal *Blautia* Is Associated with Reduced Death from Graft-versus-Host Disease. *Biol Blood Marrow Tr* **21**, 1373–1383 (2015).
24. Segata N, *et al.* Metagenomic biomarker discovery and explanation. *Genome Biol* **12**, R60 (2011).
25. Oh TG, *et al.* A Universal Gut-Microbiome-Derived Signature Predicts Cirrhosis. *Cell Metab* **32**, 878–888 e876 (2020).
26. Blacher E, Levy M, Tatrovsky E, Elinav E. Microbiome-Modulated Metabolites at the Interface of Host Immunity. *J Immunol* **198**, 572–580 (2017).
27. Perricone C, De Carolis C, Perricone R. Glutathione: a key player in autoimmunity. *Autoimmun Rev* **8**, 697–701 (2009).
28. McDonald C, Inohara N, Nunez G. Peptidoglycan signaling in innate immunity and inflammatory disease. *J Biol Chem* **280**, 20177–20180 (2005).
29. Norelli M, *et al.* Monocyte-derived IL-1 and IL-6 are differentially required for cytokine-release syndrome and neurotoxicity due to CAR T cells. *Nature Medicine* **24**, 739–748 (2018).
30. Lee DW, *et al.* Current concepts in the diagnosis and management of cytokine release syndrome. *Blood* **124**, 188–195 (2014).
31. Brudno JN, Kochenderfer JN. Toxicities of chimeric antigen receptor T cells: recognition and management. *Blood* **127**, 3321–3330 (2016).
32. Peters BA, *et al.* Relating the gut metagenome and metatranscriptome to immunotherapy responses in melanoma patients. *Genome Med* **11**, 61 (2019).
33. Matson V, *et al.* The commensal microbiome is associated with anti-PD-1 efficacy in metastatic melanoma patients. *Science* **359**, 104–108 (2018).
34. Geva-Zatorsky N, *et al.* Mining the Human Gut Microbiota for Immunomodulatory Organisms. *Cell* **168**, 928–943 e911 (2017).

35. Botticelli A, *et al.* Changes of microbiome profile during nivolumab treatment in NSCLC patients. In: *Asco* (2018).
36. Schirmer M, *et al.* Linking the Human Gut Microbiome to Inflammatory Cytokine Production Capacity. *Cell* **167**, 1897 (2016).
37. Kim YJ, *et al.* *Stenotrophomonas maltophilia* outer membrane vesicles elicit a potent inflammatory response in vitro and in vivo. *Pathog Dis* **74**, (2016).
38. Pompilio A, Crocetta V, Di Bonaventura G. *Stenotrophomonas maltophilia* mutant lacking flagella remains virulent in DBA/2N mice but is less efficient in stimulating TNF-alpha expression. *FEMS Microbiol Lett* **365**, (2018).
39. Kale SD, *et al.* "Small" Intestinal Immunopathology Plays a "Big" Role in Lethal Cytokine Release Syndrome, and Its Modulation by Interferon-gamma, IL-17A, and a Janus Kinase Inhibitor. *Front Immunol* **11**, 1311 (2020).
40. Matera G, *et al.* Procalcitonin neutralizes bacterial LPS and reduces LPS-induced cytokine release in human peripheral blood mononuclear cells. *BMC Microbiol* **12**, 68 (2012).
41. Wong MH, Chapin OC, Johnson MD. LPS-stimulated cytokine production in type I cells is modulated by the renin-angiotensin system. *Am J Respir Cell Mol Biol* **46**, 641–650 (2012).
42. Dziarski R. Recognition of bacterial peptidoglycan by the innate immune system. *Cell Mol Life Sci* **60**, 1793–1804 (2003).
43. Durie BG, *et al.* International uniform response criteria for multiple myeloma. *Leukemia* **20**, 1467–1473 (2006).
44. Rajkumar SV, *et al.* Consensus recommendations for the uniform reporting of clinical trials: report of the International Myeloma Workshop Consensus Panel 1. *Blood* **117**, 4691–4695 (2011).
45. Hu Y, *et al.* Potent Anti-leukemia Activities of Chimeric Antigen Receptor-Modified T Cells against CD19 in Chinese Patients with Relapsed/Refractory Acute Lymphocytic Leukemia. *Clin Cancer Res* **23**, 3297–3306 (2017).
46. Wang Y, *et al.* A retrospective comparison of CD19 single and CD19/CD22 bispecific targeted chimeric antigen receptor T cell therapy in patients with relapsed/refractory acute lymphoblastic leukemia. *Blood Cancer J* **10**, 105 (2020).
47. Rognes T, Flouri T, Nichols B, Quince C, Mahe F. VSEARCH: a versatile open source tool for metagenomics. *PeerJ* **4**, e2584 (2016).
48. Bolyen E, *et al.* Reproducible, interactive, scalable and extensible microbiome data science using QIIME 2. *Nat Biotechnol* **37**, 852–857 (2019).
49. Amir A, *et al.* Deblur Rapidly Resolves Single-Nucleotide Community Sequence Patterns. *mSystems* **2**, (2017).
50. Price MN, Dehal PS, Arkin AP. FastTree 2—approximately maximum-likelihood trees for large alignments. *PLoS One* **5**, e9490 (2010).

51. Bokulich NA, *et al.* Optimizing taxonomic classification of marker-gene amplicon sequences with QIIME 2's q2-feature-classifier plugin. *Microbiome* **6**, 90 (2018).
52. Douglas GM, *et al.* PICRUSt2: An improved and extensible approach for metagenome inference. *bioRxiv*, 672295 (2019).
53. Bokulich NA, *et al.* q2-longitudinal: Longitudinal and Paired-Sample Analyses of Microbiome Data. *mSystems* **3**, (2018).
54. Nueda MJ, Tarazona S, Conesa A. Next maSigPro: updating maSigPro bioconductor package for RNA-seq time series. *Bioinformatics* **30**, 2598–2602 (2014).
55. Conesa A, Nueda MJ, Ferrer A, Talón M. maSigPro: a method to identify significantly differential expression profiles in time-course microarray experiments. *Bioinformatics* **22**, 1096–1102 (2006).
56. Shannon P, *et al.* Cytoscape: a software environment for integrated models of biomolecular interaction networks. *Genome Res* **13**, 2498–2504 (2003).

Figures

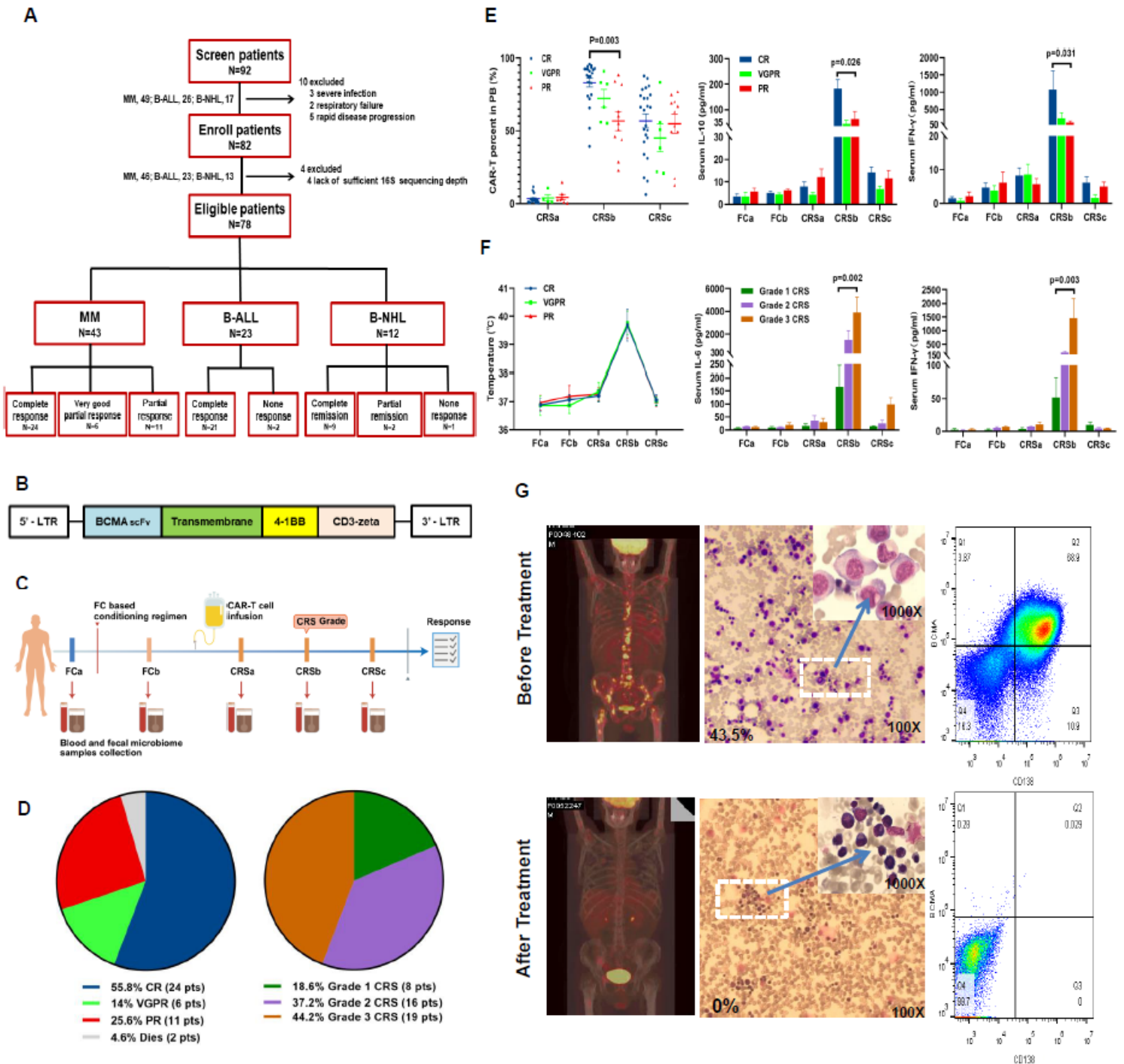


Figure 1

Trial profile and clinical response in r/r MM patients treated with CAR-T cell infusion. (A) Patient enrollment. (B) Anti-BCMA single-chain variable fragment (scFv), a hinge and transmembrane regions, and 4-1BB costimulatory moiety, and CD3 ζ T-cell activation domain. (C) Blood and fecal sample collection. (D) Clinical response; CRS grade distribution in 43 r/r MM patients. (E) Numbers of BCMA CAR-T cell percentages in PB assessed by FACS in different therapy stages after CAR-T cell infusion and serum concentrations of IL-6 and IFN- γ in different therapy stages among the CR, EPR, and PR groups. (F) Body temperature and serum concentrations of IL-6 and IFN- γ in different therapy stages among CRS

grade groups. (G) Representative MM patients with impressive antimyeloma response. Positron emission tomography-computed tomography scans before and five months after CAR-T cell treatment showing complete elimination of large number of MM bone metastases. Before receiving CAR-T cell infusion, 43.5% of bone marrow cells of the patient were plasma cells, but after 1.5 months of infusion, dramatic eradication of MM from the bone marrow was observed; and MM cells became undetectable by flow cytometry.

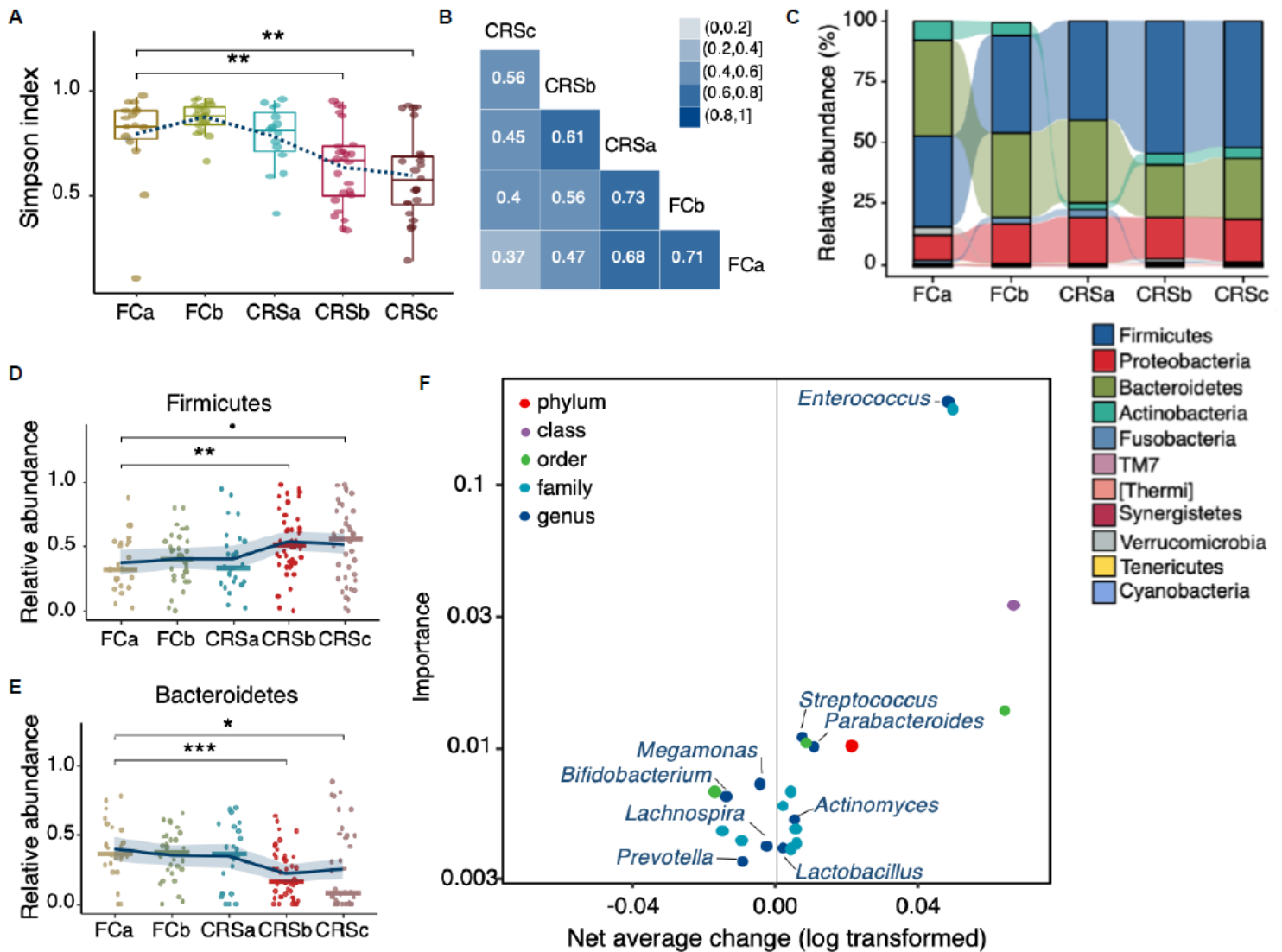


Figure 2

Changes of microbial composition during CAR-T therapy. (A) Simpson diversity indices of gut microbiome across CAR-T stages in all myeloma patients by Wilcoxon rank-sum test. (B) Pairwise Spearman correlation of OTU-level bacterial abundance across different timepoints. Rho value for each significant correlation is labelled inside box. (C) Stacked bar plot of mean phylum-level phylogenetic composition of bacterial taxa in myeloma patients across therapy stages. (D, E) Relative abundance of phyla Firmicutes and Bacteroidetes across therapy stages. Significance was assessed by Wilcoxon rank-

sum test. (F) Longitudinal analysis by Qiime2 “feature-volatility” plugin to identify taxonomic features associated with therapy stages. Important genus-level features are labelled.

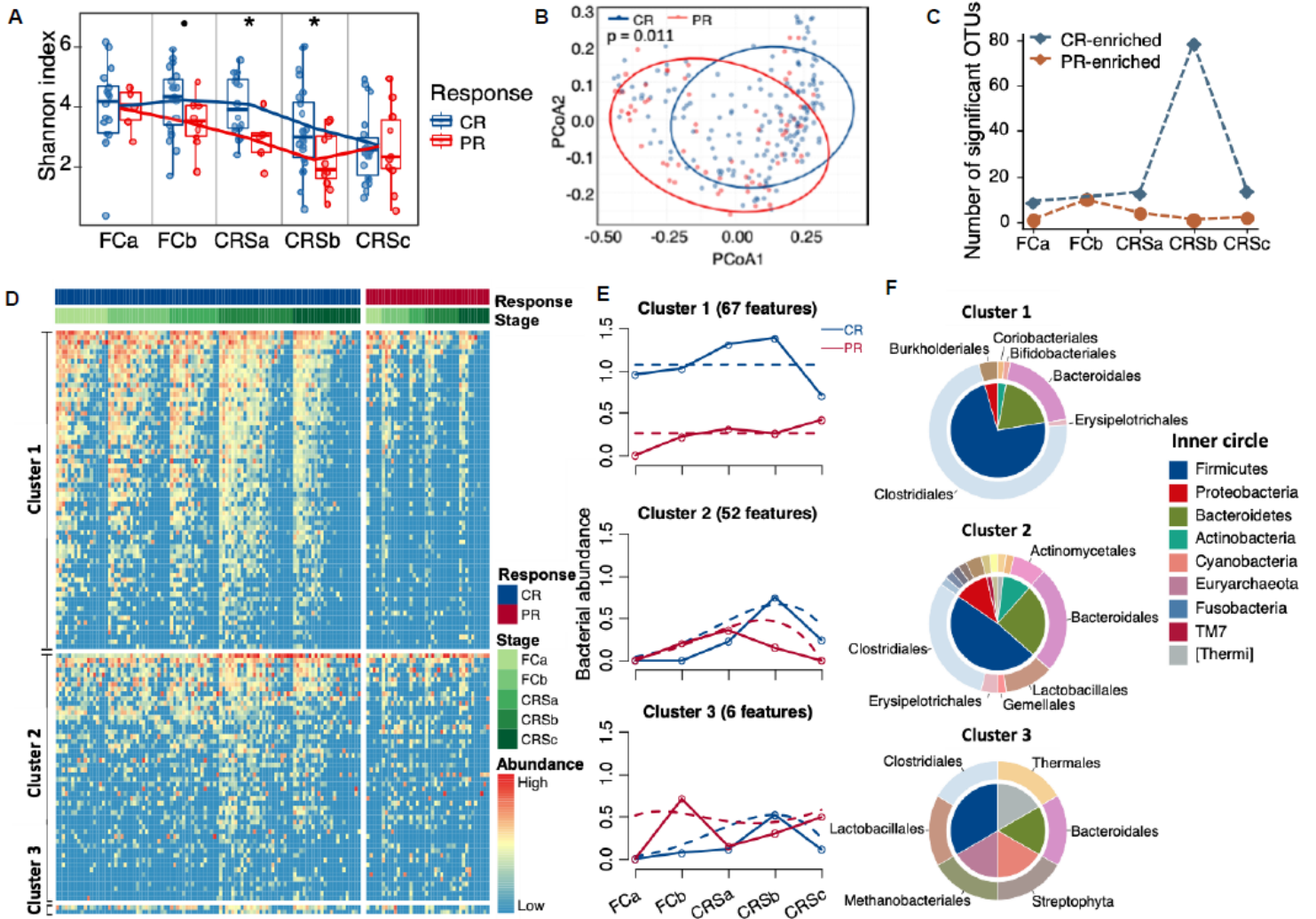


Figure 3

Association of compositional differences in gut microbiome with responses to CAR-T therapy. (A) Shannon diversity indices of gut microbiome differed between CR and PR groups across CAR-T stages. Significances were assessed by Wilcoxon rank-sum test. (B) Principal coordinate analysis of fecal samples by response using weighted UniFrac distances. (C) Summary of number of PR or CR-enriched OTUs in different therapy stages. Difference between CR and PR groups was assessed by Wilcoxon rank-sum test. P value significant cutoff was 0.05. (D) Heatmap for abundance of OTUs with significant temporal differences between CR and PR groups identified by maSigPro. Rows denote bacterial OTUs grouped into three sets according to regression coefficients and sorted by mean abundance within each set. Individual samples are organized in columns, with colored bars representing response group and therapy stage. (E) Profiles of significant gene clusters correspond to (D). Solid lines denote median profile of abundance of OTUs within cluster for each experimental group through time. Fitted curve of each

group is displayed as dotted line. (F) Phylogenetic composition of OTUs within each cluster in (D) at phylum and order levels.

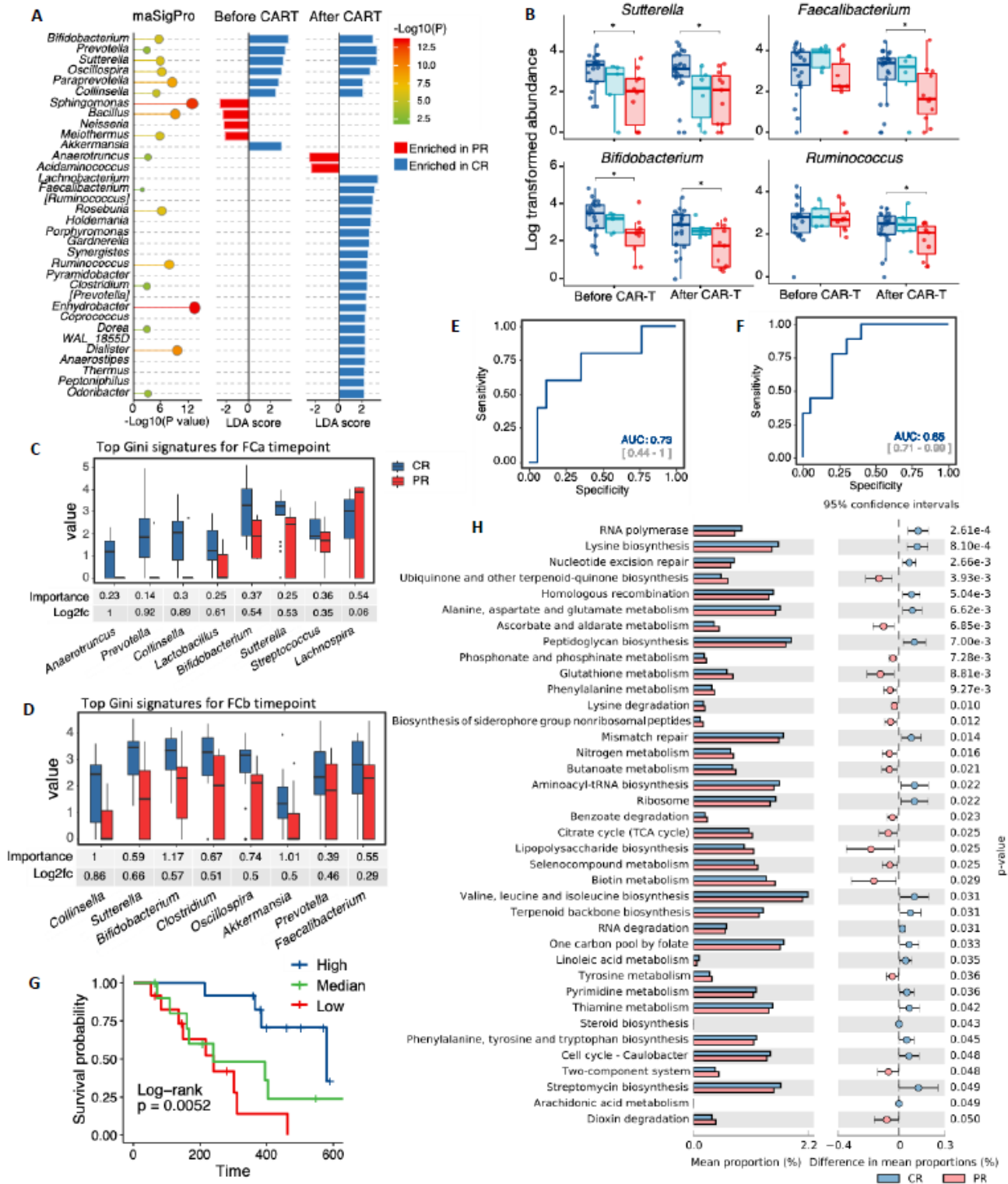


Figure 4

Determination of correlated genera with clinical response to CAR-T therapy. (A) Differentially abundant genera in CR and PR patients were identified by LefSe and maSigPro. Bar plots denote linear discriminant analysis (LDA) scores computed for differentially abundant genera in CR (blue) and PR (red) groups

using LefSe. $P < 0.05$ for Kruskal-Wallis H statistic; LDA score > 2 . Bubble plot on left marked p values from temporal group difference analysis for each genus. Bubble size and color are proportional to log-transformed p value. (B) Mean bacterial abundance (log transformed) of CR, VGPR, and PR myeloma patients before and after CAR-T cell infusion. Significances tested with Wilcoxon rank-sum test; * $p < 0.05$. (C) Relative abundance (log transformed) of top discriminative signatures at baseline (FCa) timepoint identified by RF feature selection procedure. Genera with highest scores of mean decreases in Gini were selected. Importance scores in RF classification model and fold-change levels in log₂ scale are noted below plot for each genus. Underlined genera are those identified at both baseline and post-chemotherapy stages. (D) Same as panel C for post-chemotherapy (FCb) timepoint. Only signatures enriched in CR patients are displayed. Those depleted in CR patients are displayed in Fig. S2C. (E) Receiver operating characteristic (ROC) curve of RF model using discriminatory genera as predictors for baseline timepoint. (F) Same as panel E for post-chemotherapy timepoint. (G) Kaplan-Meier (KM) plot of PFS curves by log-rank test for patients with high (dark blue), median (green), or low (red) abundance of Sutterella. Abundance of genus Sutterella was in terms of median abundance of all timepoints. (H) Differential KEGG pathways in CR and PR groups measured by Welch's t-test. Bar plot on left denotes mean proportion of each pathway in CR and PR groups. Dot plot on right depicts difference in mean proportion. Blue and red dots represent pathways enriched in CR and PR groups, respectively.

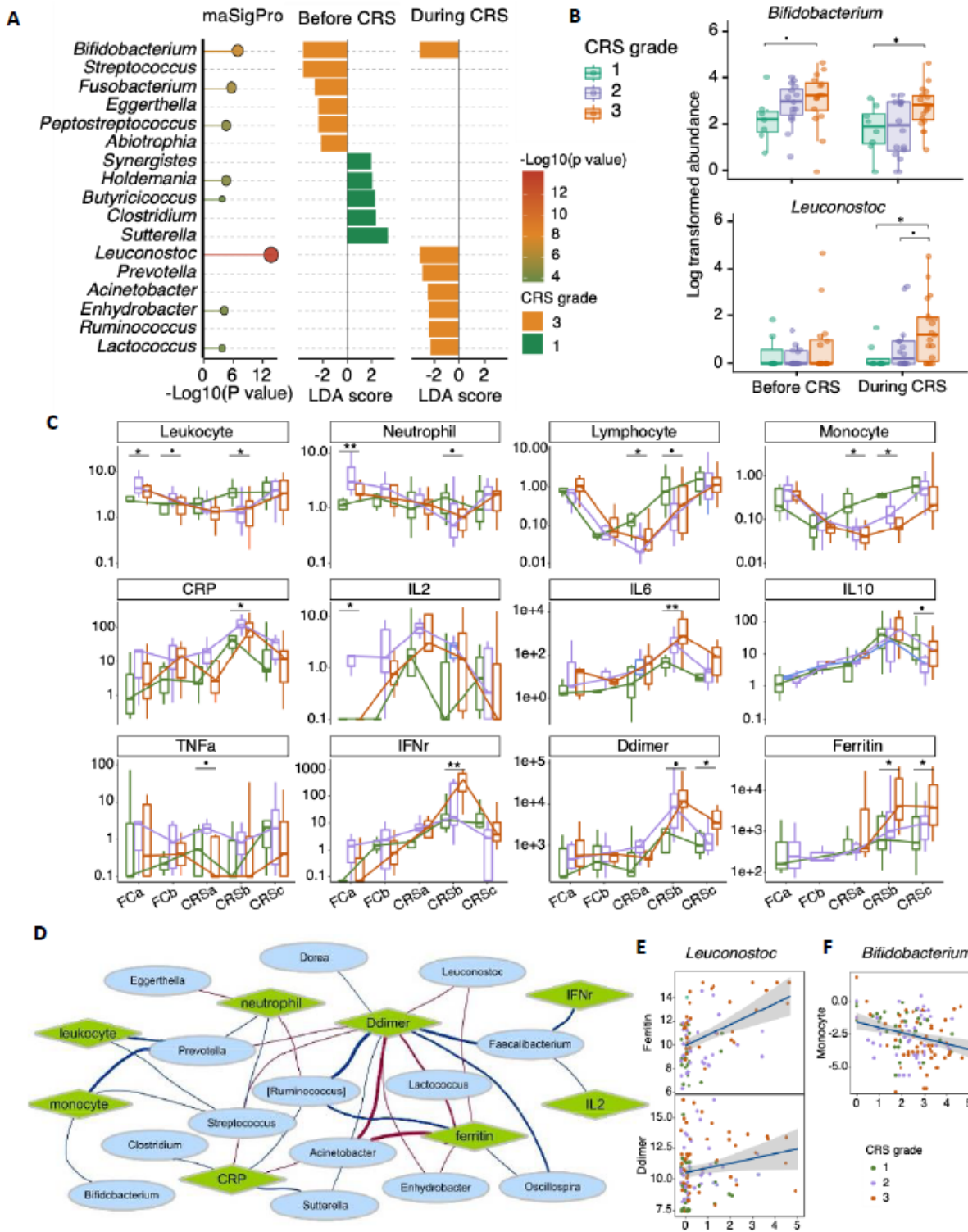


Figure 5

Compositional differences between subjects with different CRS grades. (A) Differentially abundant genera in severe (CRS = 3) and mild (CRS = 1) CRS groups identified by LefSe and maSigPro. Bar plots denote linear discriminant analysis (LDA) scores computed for differentially abundant genera in CRS grades 1 (green) and 3 (orange) groups by LefSe ($p < 0.05$ and LDA score > 2). Bubble plot on left marks p values from temporal group difference analysis for each genus calculated by maSigPro. Bubble size

and color are proportion to log-transformed p value. (B) Mean bacterial abundance in MM patients with different CRS grades before and during occurrence of CRS. Significances were assessed with Wilcoxon rank-sum test. (C) Concentrations of immune cells and inflammatory markers in different CRS grades across therapy stages. Significances were assessed by Kruskal-Wallis test. (D) Network representing correlations between gut microbes (blue nodes) and immune cells and inflammatory markers (green nodes) at $FDR < 0.2$ and $\rho > 0.2$. Red edges indicate positive correlations and blue edges negative correlations. Edge width is proportional to correlation coefficient (ρ) calculated by Spearman correlation test. Only genera identified as associated with clinical response and CRS grade were included in correlation analysis. (E) Correlation plots for *Leuconostoc* and correlated immune cells and inflammatory markers from network shown in (D). Color of dots represents CRS grades. (F) Same as (E) for *Bifidobacterium*. $p < 0.1$; * $p < 0.05$; ** $p < 0.01$.

Supplementary Files

This is a list of supplementary files associated with this preprint. Click to download.

- [naturecommunicationSupplementaryMaterial.docx](#)